Adsorption of Hydrogen Sulfide at Low Temperatures Using an Industrial Molecular Sieve: An Experimental and Theoretical Study

Amvrosios G. Georgiadis, Nikolaos D. Charisiou, Safa Gaber, Kyriaki Polychronopoulou, Ioannis V. Yentekakis, and Maria A. Goula*

Read Online

ACCESS | Metrics & More | Article Recommendations

ABSTRACT: In the work presented herein, a joint experimental and theoretical approach has been carried out to obtain an insight into the desulfurization performance of an industrial molecular sieve (IMS), resembling a zeolitic structure with a morphology of cubic crystallites and a high surface area of 590 m^2 g^{-1}, with a view to removing H_2S from biogas. The impact of temperature, H_2S inlet concentration, gas matrix, and regeneration cycles on the desulfurization performance of the IMS was thoroughly probed. The adsorption equilibrium, sorption kinetics, and thermodynamics were also examined. Experimental results showed that the relationship between H_2S uptake and temperature increase was inversely proportional. Higher H_2S initial concentrations led to lower breakpoints. The presence of CO_2 negatively affected the

desulfurization performance. The IMS was fully regenerated after 15 adsorption/desorption cycles. Theoretical studies revealed that the Langmuir isotherm better described the sorption behavior, pore diffusion was the controlling step of the process (Bangham model), and that the activation energy was 42.7 kJ mol^{-1} (physisorption). Finally, the thermodynamic studies confirmed that physisorption predominated.
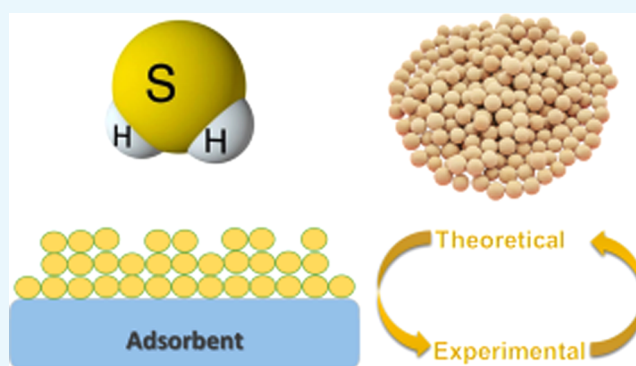
1. INTRODUCTION

Biogas is a gaseous mixture produced by methanogenic bacteria through anaerobic digestion of organic matter[1−3] and is one of the fastest growing renewable energy sources, as it can be easily and cheaply obtained, with its production increasing by approximately 184% between 2007 and 2016.[4]

Typically, raw biogas is composed of CH_4 (60−70%), CO_2 (30−40%), H_2O (5−10%), and, depending on the biomass matrix, trace amounts of other species such as H_2S (0.15−3%), NH_3 (<1%), CO (<0.6%), siloxanes, carbonyls, terpenes, and aromatic or halogenated compounds.[3−7] Biogas upgrading for increasing its calorific value involves specific steps, starting with H_2O condensation, desulfurization (e.g., removal of toxic and corrosive H_2S), and CO_2 sequestration based on different universally established and commonly used technologies including physisorption and/or chemisorption, membrane or cryogenic separation, and by chemical or biological treatment.[3,8−10]

To remove sulfur compounds (i.e., H_2S), chemical, biological, and physical methods are applied.[3,11] For example, acid and basic compounds (i.e., metal oxides, NaOH) can promote H_2S removal through oxidation or/and acid−base reactions.[12,13] However, the practicality of these techniques is questionable owing to environmental repercussions (secondary

wastes).[14] Even though biological processes can achieve a high degree of desulfurization, they require high capital investment.[15,16] Physical methods include H_2O scrubbing, membrane separation, and dry processes.[17]

Typically, in dry processes, a solid frame and a gaseous stream interact and various reactions can take place, depending on the properties of the solid frame. Dry desulfurization can be realized by employing hydro-desulfurization, selective catalytic oxidation, and adsorption.[18] Hydro-desulfurization is an efficient desulfurization method, but it is energy-intensive as high hydrogen pressure and temperature are needed.[19] Selective catalytic oxidation also requires high temperatures and the addition of air, while it also leads to SO_2 production.[20] The integration of the above technologies into a plant requires extra costs, which are not viable for small-scale applications. In contrast, adsorption can be applied for both large- and small-

scale applications as it can achieve increased desulfurization performance even at low concentrations and temperatures.[18,21]

That said, efforts to develop materials for gas sweetening applications that meet the strict product requirements and environmental regulations are intense.[22] Different materials have been used thus far to remove H_2S from biogas, including metal−organic frameworks (MOFs), activated carbons, metal oxides, and zeolites.[23] Searching through the available literature, it becomes apparent that the best-performing materials reported to date are activated carbons with H_2S uptake up to 300 mg g^{-1} at ambient temperature.[24] Nevertheless, activated carbons suffer from poor regenerability.[23] Regarding MOFs, Hamon et al.[25] reported H_2S uptake from 170 to 340 mg g^{-1}, depending on the type of metal-organic framework (MOF) tested. However, these capacities were achieved at equilibrium under high pressure, which typically results in higher capacities than those obtained at dynamic conditions. In addition, MOFs have yet to have a commercial impact, mostly due to stability and cost-effectiveness issues.[23] Mixed-metal oxides, mostly based on Zn, Fe, and Mn, or combinations of those, outperform, in terms of sulfur removal efficiency, single-metal oxides, but they are inferior to other conventional adsorbents.[26] Zeolites gained considerable attention due to their high selectivity and affinity toward polar compounds (i.e., H_2S) as well as their high stability. Along these lines, a number of works consider that zeolites are the most appropriate H_2S adsorbents for industrial use. However, in most cases, they need energetically demanding regeneration processes (typically above 450 °C).[17]

Zeolites, also referred to as molecular sieves,[27] are microporous crystalline aluminosilicates with a uniform pore structure that show ion-exchange behavior.[28] Generally, zeolites containing lower Si/Al ratios tend to adsorb polar substances and are more hydrophilic, while zeolites with higher Si/Al ratios are hydrothermally stable and more hydrophobic in comparison and thus can potentially favor the adsorption of nonpolar molecules.[29,30]

Thence, a fair amount of scientific works delved deeper into zeolite-based H_2S adsorption processes and retention mechanisms. Karge et al.[31] investigated H_2S adsorption on Na-Y and Na-X zeolites, paying attention to the Si/Al ratio. The authors reported reversible H_2S adsorption for Si/Al > 2.5 (Na-Y) and dissociative adsorption of H_2S for Na-X zeolite. Cruz et al.[32] tested activated carbons, 13X and Y sodium zeolites, silica gel, and clay pillared with aluminum oxide to capture H_2S at low concentrations from a confined atmosphere. Melo et al.[33] compared the H_2S adsorption capacities of Zinox 298 (88% ZnO) and 13X zeolite aiming at natural gas sweetening and found that 13X outperformed Zinox 298. Barelli et al.[34] also studied the desulfurization performance of a 13X zeolite treated with Cu ions (13X Ex-Cu) by impregnation or ion exchange. Alonzo-Vicario et al.[35] observed higher H_2S adsorption capacity for Clinoptilolite (natural zeolite) in comparison to that of synthetic ones (5A, 13X) by deploying pressure swing adsorption. Tomadakis et al.[36] deployed three different types of zeolites (4A, 5A, and 13X) to separate high-content H_2S/CO_2 mixtures via pressure swing adsorption and pointed out that 5A and 13X presented higher selectivity compared to 4A for adsorbing H_2S over CO_2. Micoli et al.[37] tried to remove H_2S from biogas for fueling molten carbonate fuels cells (MCFCs) by means of zinc-modified zeolites prepared by ion exchange or impregnation and found that modified materials were superior in terms of H_2S capture.

Yokogawa et al.[38] used LTA (zeolite-A), MFI (ZSM-5), Ag-grafted LTA, and Ag-grafted MFI to remove volatile sulfur compounds (VSCs) and reported that the concentration of H_2S zeroed for the Ag-doped zeolites (i.e., after 4 h for Ag-LTA and after 8 h for Ag-MFI). Sigot et al.[39] reported that the NaX zeolite (Si/Al = 1.4) failed to regenerate following H_2S exposure. Similarly, Yang et al.[40] explored the regeneration potential of 13X zeolite, which was used for the synchronous removal of H_2S and SO_2 in the presence of high H_2O concentrations, and concluded that after several adsorption−regeneration cycles the material lost part of its adsorption capacity. Liu et al.[41] studied a 4A zeolite synthesized from attapulgite to remove H_2S from different industrial gases at low temperatures.

Bearing in mind the aforementioned discussion, chemisorption can satisfy the demand for the selective capture of H_2S; however, the downside is that it causes the formation of irreversible bonds that compromises the regeneration potential and eventually leads to the substitution of the sorbent.[42,43] On the other hand, a reversible process can be achieved in physisorption since it is dominated by weak van der Waals forces and electrostatic interactions, but the selective adsorption of H_2S seems to pose an insurmountable challenge.[44]

The objective of this study is to determine the adsorption performance of the industrial molecular sieve (IMS) in H_2S removal at different temperatures, H_2S inlet concentrations, gas matrixes, and adsorption/desorption cycles. In addition, effort was spent in investigating the adsorption equilibrium, sorption kinetics, and thermodynamic parameters to further elucidate the mechanisms that govern the adsorption process. It is pointed out that both the activation and the desorption process were carried out at 200 °C, which is a relatively low temperature in comparison to those presented in the literature. From the results obtained, it is argued that the material tested may provide a realistic and cost-effective solution with direct industrial applicability.

2. RESULTS AND DISCUSSION

2.1. Structural Overview of the IMS Adsorbent. The crystallinity of the IMS adsorbent was studied using X-ray diffraction (XRD). High-intensity peaks were revealed, demonstrating the high crystallinity of the material (Figure 1).
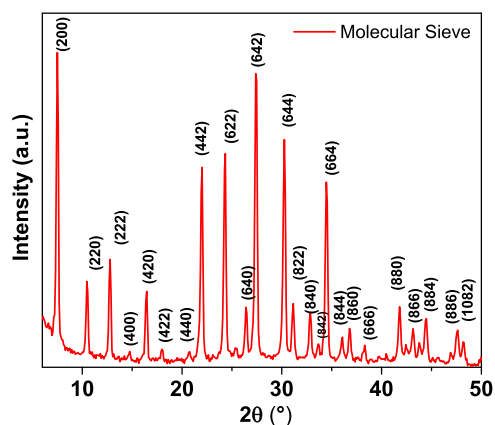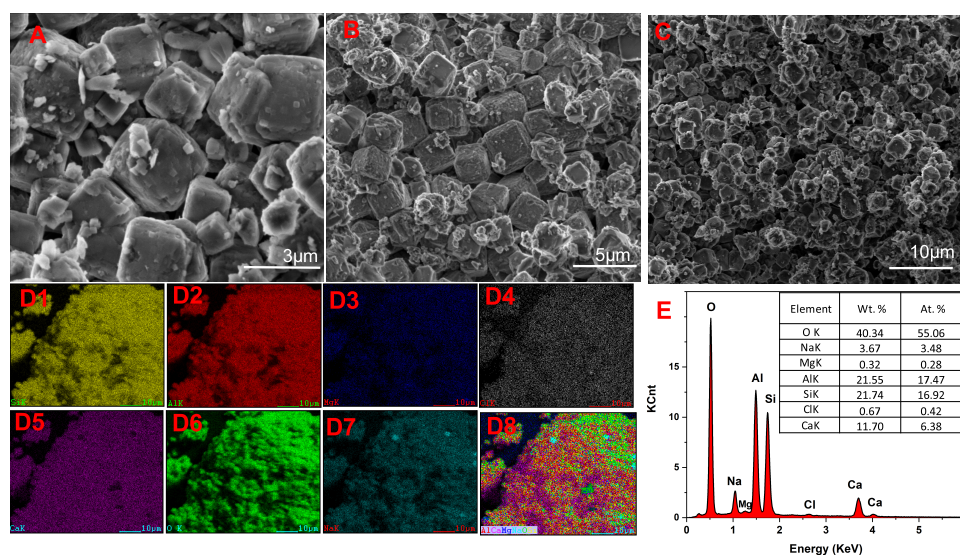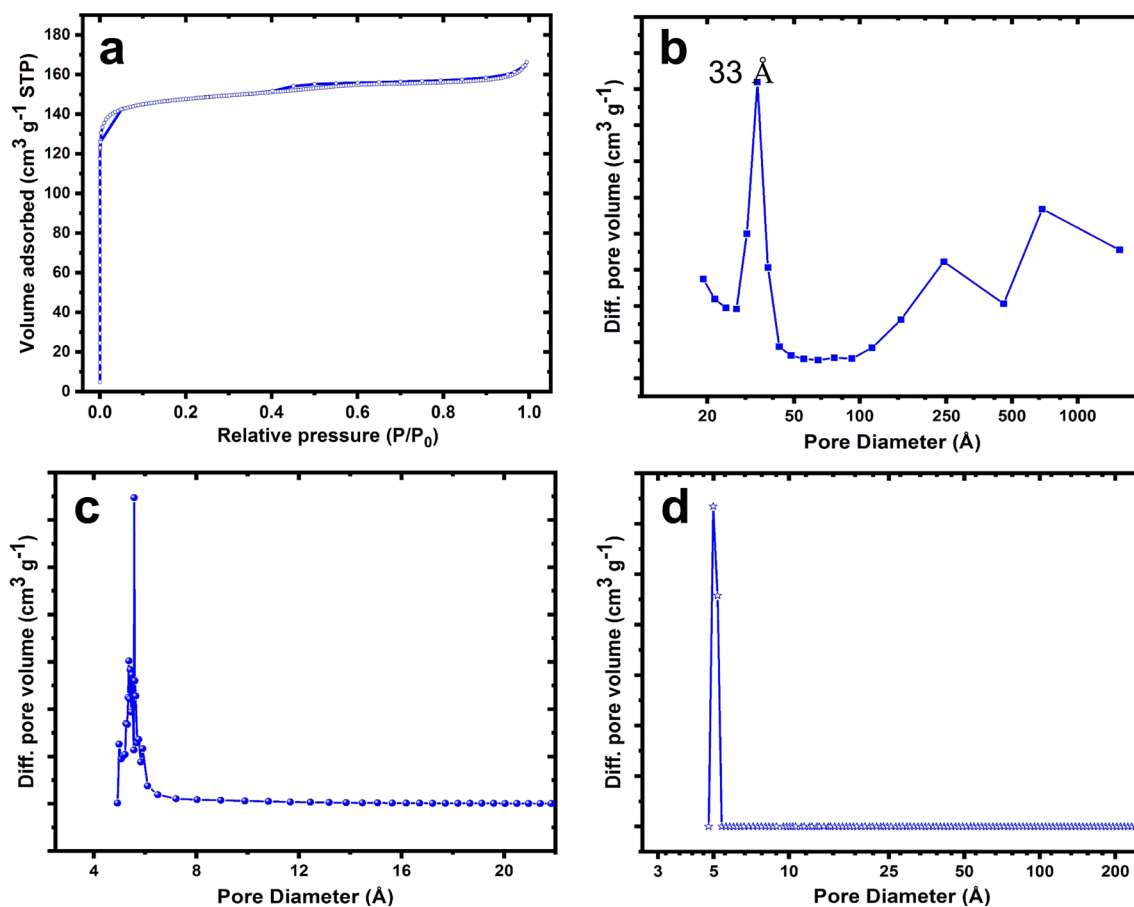

Figure 1. XRD pattern of the IMS adsorbent.

Figure 2. (A−C) SEM microphotographs obtained at different magnifications, (D1−D8) EDX elemental mapping, and (E) EDX analysis over the IMS adsorbent.

Figure 3. (a) N_2 adsorption−desorption isotherm and pore size distribution, obtained over the IMS adsorbent using the BJH (b), HK (c), and NLDFT (d) methods.

Based on a careful examination of the peaks' position, as well as their relative intensity ratios, the structure closely resembles that of an LTA-type zeolite (3A or 4A).

More structural techniques are needed to classify the precise structure of the zeolite (e.g., ^{29}Si-ssNMR), which is out of the scope of this work. Scanning electron microscopy (SEM)

studies showed that the IMS material is composed of very well-shaped crystallites with a cubic morphology (Figure 2). The crystallites possess truncated edges and rather smooth surfaces, while their size is approximately 1.5−2 μm (Figure 2A,B). Energy-dispersive X-ray spectrometry (EDX) elemental analysis showed that the Si/Al ratio is 0.97, very close to 1,

which is typical for the LTA-type zeolite due to the alternating alumina and silica tetrahedra. In addition to the frame elements (Si, Al, O), Na, Ca, and traces of Mg were also found. The N_2 adsorption–desorption isotherm (Figure 3a) obtained over the IMS solid adsorbent is a typical type I isotherm, according to the IUPAC classification, where high adsorption of N_2 takes place at low relative pressures. From the pore size distribution obtained using the Barrett–Joyner–Halenda (BJH) method (Figure 3b), the main peak is centered at 3.3 nm, which suggests, to some extent, the presence of mesopores; this might be due to the dealuminated commercial samples or interparticle porosity. However, based on the Horvath–Kawazoe (HK) pore size distribution, the sample contains mostly micropores with an average pore size of 5.5 nm (Figure 3c); this is in agreement with the nonlocal density functional theory (NLDFT) pore size distribution, which clarifies that the IMS contains mostly micropores with an average pore size of 5.0 nm (Figure 3d). The specific surface area was found to be 590 m^2 g^{-1} (Table 1).

Table 1. Surface and Textural Properties of Zeolite

parameter	value
sample	IMS
surface area	590 m^2 g^{-1}
pore volume	0.25 cm^3 g^{-1}
average pore size	1.73 nm
external surface	53 m^2 g^{-1}
micropore area	537 m^2 g^{-1}
micropore volume	0.2 cm^3 g^{-1}

2.2. Experimental Studies. *2.2.1. Effect of Temperature.* The effect of temperature was evaluated between 25 and 100 °C. The gas matrix consisted of Ar and H_2S with an inlet concentration for the latter of 3000 ppm (h/D = 2.22, Q_{total} = 100 mL min^{-1}). As can be observed in Figure 4, the H_2S breakthrough capacity decreased with an increase of the adsorption temperature, which indicates that physisorption occurs.
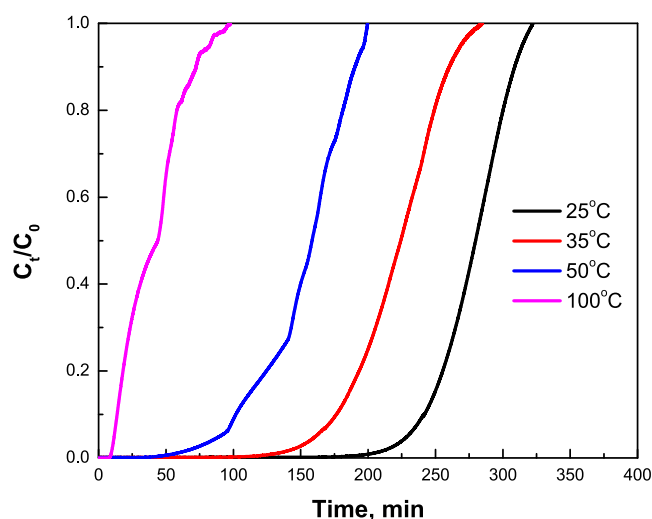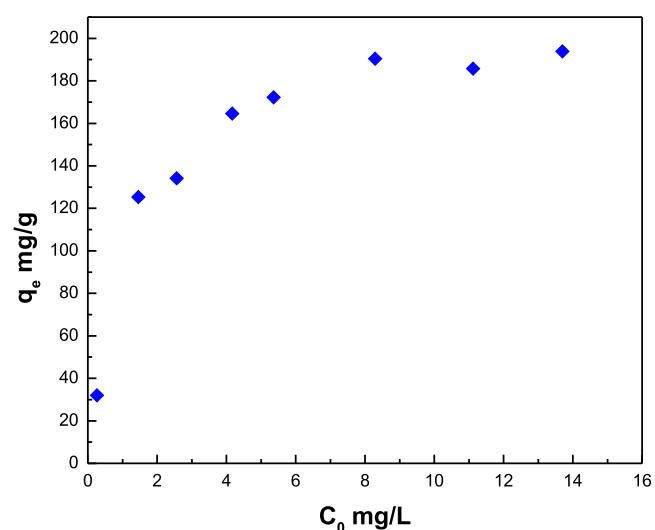
For example, H_2S uptake dropped by 24.0% when the temperature was raised from 25 to 35 °C (i.e., from 164.5 to 122.8 mg g^{-1}). A further decrease of 30.0 and 82.0% occurred when the adsorption temperature was raised from 35 to 50 °C (i.e., from 122.8 to 86.1 mg g^{-1}) and from 50 to 100 °C (i.e., from 86.1 to 15.3 mg g^{-1}), respectively. These results can be explained by the fact that the H_2S adsorption process is largely dominated by electrostatic interactions (physical adsorption).[45] As physical adsorption is exothermic in nature, an increase in temperature can compromise the process. In this regard, Liu et al.[41] found that the desulfurization performance was negatively affected by increasing temperature due to the exothermic nature of the reaction, leading to lower H_2S capture at 75 °C (6.5 mg g^{-1}) in comparison to that at 50 °C (8.36 mg g^{-1}). Yaşyerli et al.[46] explored the desulfurization performance of a clinoptilolite at different temperatures and found that it decreased by increasing temperature (from 87.0 mg g^{-1} at 100 °C to 30.0 mg g^{-1} at 600 °C). Asaoka et al.[47] also reported that increasing the adsorption temperature can promote chemisorption and yet be not conducive to physisorption.

2.2.2. Effect of H_2S Concentration. The effect of the H_2S inlet concentration was probed for the IMS in the range of 200–10 000 ppm at 25 °C as this was the optimum adsorption temperature identified (h/D = 2.22, Q_{total} = 100 mL min^{-1}). Generally, higher initial H_2S concentrations led to the decrease of breakpoint (i.e., from 612 min at 200 ppm to 69 min at 10 000 ppm), which can be ascribed to the effective pore diffusivity decrease with increasing initial H_2S content.[48]

The highest H_2S adsorption capacity was 193.3 mg g^{-1} and was obtained when the H_2S concentration was 10 000 ppm. The lower H_2S uptake was derived for an inlet H_2S concentration of 200 ppm (32.0 mg g^{-1} adsorbed for 839 min of saturation time). It is worth noticing that the isotherm reached a plateau (isotherm type I), as shown in Figure 5, suggesting that this material retained the maximum amount of H_2S molecules possible, and a further increase in the inlet concentration is futile. The slight decrease in adsorption capacity at 8000 ppm is probably ascribed to experimental error.

Figure 4. H_2S adsorption breakthrough curves for IMS at 25, 35, 50, and 100 °C in a fixed-bed quartz reactor (1 atm, 3000 ppm H_2S in an Ar stream, flow rate 100 mL min^{-1}).

Figure 5. H_2S uptake for the different H_2S concentrations tested (equilibrium isotherm).

The reversible type I isotherm, usually referred to as the Langmuir isotherm, is given by microporous materials having relatively small external surfaces, such as zeolites and activated carbons, without interactions between the species getting adsorbed.[49] A more extensive discussion for isotherm models is subsequently presented.

Table 2 summarizes the results obtained in the range of 200−10 000 ppm, illustrating the H_2S adsorption capacity.

Table 2. Effect of H_2S Concentration on Adsorption Capacity

H_2S concentration (ppm)	equilibrium capacity (mg g^{-1})	equilibrium capacity (mg m^{-2})
200	32.0	0.054
1000	125.3	0.212
2000	134.2	0.227
3000	164.5	0.279
4000	172.2	0.292
6000	190.4	0.323
8000	185.5	0.314
10 000	193.9	0.329

Generally, higher influent concentrations can result in increasing the driving force along the pores and consequently in higher adsorption capacities, which is evidenced by steeper breakthrough curves and a faster equilibrium.[50] Resultantly, increasing the inlet H_2S concentration, at a constant flow rate, causes shorter breakthrough times (Figure 6) due to faster saturation of the active sites responsible for H_2S adsorption.
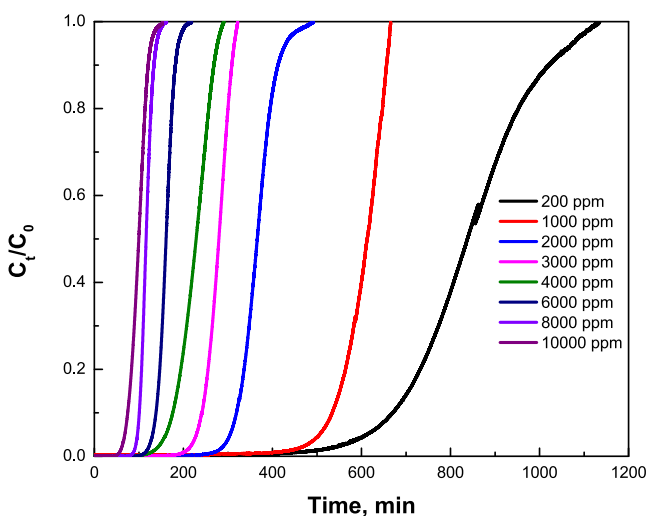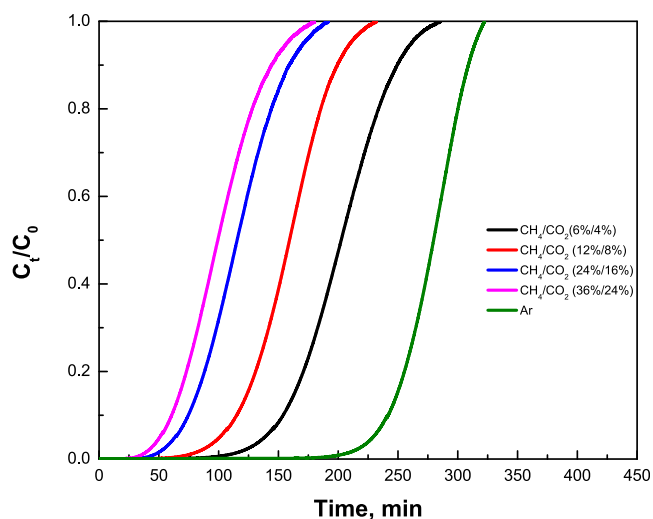

Figure 6. H_2S adsorption breakthrough curves for IMS at different inlet concentrations in a fixed-bed quartz reactor (25 °C, 1 atm, flow rate 100 mL min^{-1}).

Conversely, lower influent concentrations can lead to lower mass-transfer flux from the bulk gas to the surface of the materials owing to the decreased driving force.[51] Sometimes, as the literature shows, in dynamic adsorption tests, the effect of driving force and mass-transfer flux is low on the grounds that it is limited by the rate of molecular diffusion into deeper pores.[52,53]

2.2.3. Effect of Gas Matrix Composition. The influence of the presence of CO_2 and CH_4 on H_2S adsorption capacity was also evaluated (inlet H_2S concentration = 3000 ppm, T = 25

°C, h/D = 2.22, and Q_{total} = 100 mL min^{-1}), and the breakthrough curves obtained are presented in Figure 7; it is noted that the CH_4/CO_2 molar ratio used was equal to 1.5, simulating typical biogas concentrations.

Figure 7. H_2S adsorption breakthrough curves for IMS at different gas matrixes in a fixed-bed quartz reactor (25 °C, 3000 ppm of H_2S, 1 atm, flow rate 100 mL min^{-1}).

As strong selective interactions can be developed between the cations in aluminosilicate zeolites and the targeted polar molecules (i.e., H_2S and CO_2), IMS can be considered an appropriate choice to perform this set of adsorption runs.[9] Indeed, the IMS seemed to not retain nonpolar CH_4 molecules with tetrahedral geometry and no permanent electric dipole moment.[39,54] In general, lower molecular weights (e.g., CH_4 = 16.04, H_2S = 34.1, CO_2 = 44.01) are associated with weaker London forces. This is also the case for molecules that are not easily polarized.[9] The kinetic diameters of the CH_4, H_2S, and CO_2 molecules are 3.8, 3.6, and 3.3 Å, respectively, rather close to each other. On the other hand, polarizability among the three gases of interest varies as follows: CO_2 (2.9 × 10^{-24} cm^3) > CH_4 (2.6 × 10^{-24} cm^3), whereas for H_2S it is 3.6 × 10^{-24} cm^3.[55] At the same time, one source of polarizability of the IMS can be the bridged OH groups (Si-(OH)-Al), where the H is more acidic compared to the Si-OH (silanol) groups. Thus, it seems that the polarizable frame of the adsorbent has good affinity for the polarizable H_2S molecule.

On the other hand, the H_2S adsorption capacity was significantly reduced in the presence of high CO_2 concentration, as the H_2S uptake decreased from 164.5 mg g^{-1} adsorbent (CO_2-free gas matrix) to 119.0 mg g^{-1} adsorbent (6% CO_2 in the gas matrix), which corresponds to a 28.0% drop. Increasing the percentage of CO_2 to 12% and then to 24 and 36% led to further decreases in the H_2S uptake on IMS to 92.1, 67.5, and 57.7 mg g^{-1}, respectively, corroborating the antagonistic relationship between these gases. Here, the acidic nature of both CO_2 and H_2S should be mentioned, which supports their competition for the same adsorption sites. Yet, the polarizable frame of IMS retained a decent H_2S adsorption capacity, meaning that this adsorbent can be considered as a candidate for dry desulfurization processes.

As has been reported in the literature, H_2S removal via physical adsorption in the presence of CO_2 is to a great extent an insuperable challenge.[54,56] Low H_2S selectivity engenders a

synchronous saturation sorption of both H_2S and CO_2. The same phenomenon was observed for other porous adsorbents as well, such as silica gel and activated carbons. Therefore, physisorption cannot gratify demands for highly efficient CO_2/H_2S separation in comparison to chemisorption,[57] where strong chemical bonds (covalent bonds) can be formed between the metal and H_2S.[58]

2.2.4. Effect of Adsorption/Desorption Cycles. Finally, adsorption/desorption tests were carried out for 15 cycles to investigate the stability of IMS following H_2S exposure.

The tests were performed using the following operating conditions: inlet H_2S concentration = 3000 ppm, T = 25 °C, h/D = 2.22, and Q_{total} = 100 mL min⁻¹. The desorption temperature was 200 °C. It is noted that no activation was carried out after the first cycle in this series of experiments and that the same sorbent was employed for all of the adsorption runs. It was observed that the H_2S uptake of the IMS was not significantly affected by the adsorption/desorption cycles, ranging from 0.236 to 0.251 mg m², and the small deviations are within the experimental error. Specifically, the reproducibility is expressed by confidence limits of the results for a confidence level of 95%.

The bar chart (Figure 8) designates that the adsorption capacities at equilibrium were almost the same, highlighting
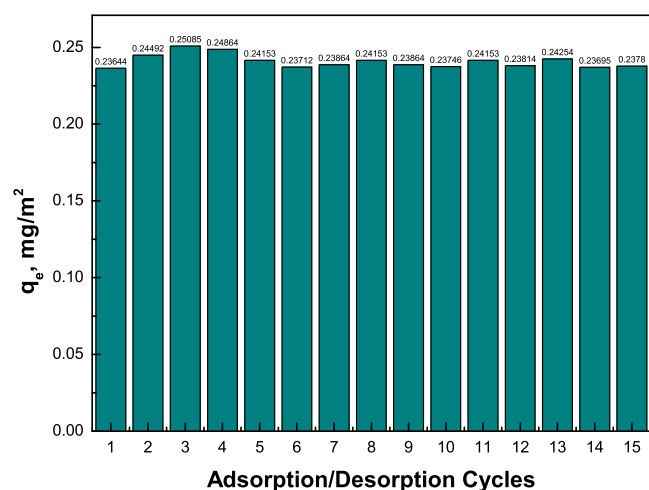
Figure 8. H_2S uptake, at equilibrium, for 15 adsorption/desorption cycles using IMS, in a fixed-bed quartz reactor (25 °C, 3000 ppm of H_2S, 1 atm, flow rate 100 mL min⁻¹).

the reversibility of the process. This reversible process was expected since the H_2S molecules were bound into IMS through a combination of electrostatic interactions, without forming chemical bonds (physisorption).[59]

2.2.5. Mechanistic Considerations of H_2S Adsorption on the IMS. The basic steps that are involved in H_2S adsorption on the IMS (zeolite-type adsorbent) are as follows, in good agreement with the literature:[26,60] (a) H_2S adsorption on the surface: $H_2S(g) \rightarrow H_2S(s)$; (b) dissolution of H_2S in the pore-bound water: $H_2S(s) \rightarrow H_2S(aq)$; and (c) dissociation of the H_2S while in the water film: $H_2S(aq) \rightarrow HS^-(aq)$.

Parameters investigated above have a pivotal role in H_2S adsorption. In particular, porosity, pore size distribution, and adsorption kinetics are crucial for step (a) in the mechanism. The presence of bonded water in the pores is also crucial, as the amount of water there should be just enough to allow film formation but not high enough to fill the pores. Increase in the

adsorption temperature lessens the water film and thus the H_2S capacity, as demonstrated above. The presence of Ca, Na, and Mg in the adsorbent (EDX studies above) seems to be crucial for step (c), as those cations contribute to the alkalinity of the zeolite-type adsorbent and they adjust the pH in the water film at levels that they boost the H_2S dissolution; based on the two H_2S acidity constants, a pH value between those two values would be sufficient, i.e., pK_{a1} = 7.2 and pK_{a2} = 13.9.[60]

The presence of biogas-related compounds, such as CO_2 and CH_4, can affect the H_2S adsorption as proved above. CO_2 seems to have a larger impact due to the higher adsorption capacities of zeolites toward CO_2 compared to CH_4,[1616] leading eventually to carbonation. In particular, the presence of CO_2 suppresses the H_2S dissociation in the water film due to pH drop, so H_2S is maintained in its molecular form rather than in its HS^- form.

2.3. Theoretical Studies. *2.3.1. Equilibrium Studies.* At this point, to analyze the equilibrium adsorption data, four different adsorption models were applied (i.e., Langmuir, Freundlich, Dubinin–Radushkevich (DR), and Temkin) at ambient temperature, which is the temperature in which the adsorbent exhibited it highest H_2S adsorption capacity. It is interesting to note that the linearized forms of these kinetic equations have been frequently used to fit the equilibrium adsorption data and to calculate the parameters needed for each occasion.[61–63] Nevertheless, the linearization process may provide inaccurate estimations of the parameters (i.e., propagate errors to the independent/dependent variables).[64] Thereby, we tapped into nonlinear methods, which can afford more precise results.

The Langmuir model assumes that a certain number of adsorption sites can be occupied on the surface of the adsorbent; each site can be dwelled by on a molecule only, which is monolayer adsorption, and the energy of this process is constant, and no interaction between the adsorbed molecules on neighboring adsorption sites takes place. The model can be expressed by the following equation[65]

$$q_e = \frac{K_L \, q_{max} \, C_e}{1 + C_e \, K_L} \tag{1}$$

where q_e and C_e are the H_2S uptake and concentration at equilibrium, respectively, K_L is the Langmuir isotherm constant related to the binding energy, and q_{max} is the theoretically calculated adsorption capacity of H_2S. However, in microporous materials, the characteristic form of the Langmuir isotherm (type I) is owing to the micropore volume-filling process and not the monolayer surface coverage.[66] Adsorption tests showed that this model is suitable for describing the experimental data, with an R^2 value of 0.978. The maximum calculated adsorption capacity was 210.7 mg g⁻¹, which was considerably close to the one obtained experimentally.

The Freundlich isotherm is applicable to adsorption processes that take place on heterogeneous surfaces.[67] This model describes both mono- and multilayer adsorption, as well as explains that the material has surfaces of varied affinities or adsorption on heterogeneous surfaces.[68] The Freundlich isotherms can be expressed by the following equation[69]

$$q_e = K_F \, C_e^{1/n} \tag{2}$$

where K_F and n signify the approximate indicators of adsorption capacity and intensity of adsorption, respectively. Generally, the higher the n value, the more active the

interaction between the adsorbate and the adsorbent.[70] However, this model does not fit well with the experimental results ($R^2 = 0.866$).

The Temkin model was also applied for equilibrium description at the best adsorption temperature (room temperature). This model describes the adsorbent−adsorbate interactions, and it can be described by the following equation[71]

$$q_e = \frac{R\,T}{B_T}\ln(A_T\,C_e) \qquad (3)$$

where A_T (L mg^{-1}) is the equilibrium binding constant and B_T (J mol^{-1}) is the Temkin constant associated with the heat of adsorption. The Temkin constant value was estimated at 0.0603 kJ mol^{-1}. It has been mentioned that for heat sorption values below 20 kJ mol^{-1}, physical adsorption predominates.[59] The R^2 value was 0.961 and provided a good fit to the experimental data.

The DR model is applied to describe the adsorption in microporous materials. It considers that multilayer adsorption transpires and that the adsorbate is captured due to van der Waals forces, giving the maximum monolayer layer adsorption capacity.[72] The DR model can be reflected by the following equation[71]

$$\ln q_e = \ln q_m - K_{DR}\,\epsilon^2 \qquad (4)$$

where K_{DR} is the constant related to the mean free energy of adsorption, q_m is the maximum H$_2$S uptake, and ϵ is the Polanyi potential, which can be derived from the following equation[61]

$$\epsilon = RT \ln(1 + 1/C_e) \qquad (5)$$

Meanwhile, the mean free energy of adsorption, E_M, can be calculated from the value of K_{DR} applying the following equation[61]

$$E_M = \frac{1}{(2K_{DR})^{0.5}} \qquad (6)$$

The model gave an R^2 value of 0.901, which specifies that H$_2$S may be adsorbed due to van der Waals forces. From the DR equation and according to the value of the free energy, an adsorption process may be categorized as (i) physisorption, when $E_M < 8.0$ kJ mol^{-1}; (ii) ion exchange, when $E_M = 8.0–16.0$ kJ mol^{-1}; and (iii) chemisorption, when $E_M > 16.0–400$ kJ mol^{-1}.[61]

The E_M value in this adsorption process was 1.522 kJ mol^{-1}. It corroborates that physical adsorption prevails as both the adsorption process and concentration of both the adsorbate and adsorbent are involved in the rate-determining step.

Resultantly, the Langmuir model was the most suitable model for describing H$_2$S adsorption into IMS, followed by, according to the R^2 value, Temkin > DR > Freundlich. More details are available in Table 3 and Figure 9.

2.3.2. Kinetic Studies. To delve deeper into the mechanism of gas-phase H$_2$S adsorption on IMS and potential rate-controlling steps, such as mass transport and chemical reaction process, four different kinetic models have been used by employing the data derived from H$_2$S adsorption runs, namely, the intraparticle diffusion (Weber−Morris) model, Bangham's model, the pseudo-first-order (PSO) model, and the pseudo-second-order (PFO) model. In line with the equilibrium

Table 3. Equilibrium Parameters of H$_2$S Adsorption

Langmuir	value	Freundlich	value
R^2	0.978	R^2	0.866
K_L (L mg^{-1})	0.811	K_F (mg$^{1-1/n}$ g^{-1} L$^{1/n}$)	98.01
$q_{e,cal}$ (mg g^{-1})	210.7	$1/n$	0.29
Temkin	value	DR	value
R^2	0.961	R^2	0.901
A_T (L mg^{-1})	10.50	K_{DR} (mol^2 kJ^{-2})	2.2×10^{-7}
B_T (kJ mol^{-1})	0.06047	E_M (kJ mol^{-1})	1.522
		$q_{e,cal}$ (mg g^{-1})	181.4
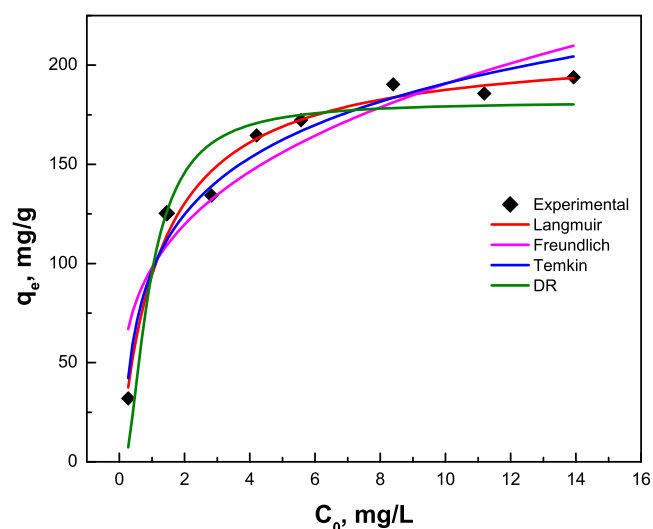
Figure 9. Isotherms of Langmuir, Freundlich, Temkin, and Dubinin−Radushkevich at ambient temperature.

studies, the optimization procedure was carried out by nonlinear fitting methods.

To identify whether intraparticle diffusion controls the process, one of the most widely used approaches for an approximate description of the adsorption is the Weber−Morris model, which can be expressed by the following equation[73]

$$q_t = k_{WM}\,t^{0.5} + C \qquad (7)$$

where k_{WM} is the Weber−Morris constant and C is related to the mass transfer across the boundary layer.

According to this model, the transitory uptake of the adsorbed gas varies nearly proportionately with the square root of time for most adsorption processes,[74] which provides an indication of the thickness of the boundary level.[61] The Weber−Morris approximation tries to identify the rate-controlling steps that took place during the adsorption by considering the initial surface adsorption and following intraparticle diffusion effects.[75]

Bangham's model can be employed to investigate whether the pore diffusion solely controls the adsorption process and can be presented as follows[76]

$$q_t = q_e\,[1-(\exp(-k_b\,t^n))] \qquad (8)$$

where k_b (min^{-n}) and n are Bangham's constants, while q_t and q_e (mg g^{-1}) present the amount of adsorbed H$_2$S at time t (min) and at equilibrium time, respectively.

This model is extensively applied as it is common for pore diffusion to be the controlling step in adsorption processes.[48]

The H_2S gas uptake into IMS may be considered as a pseudo-first-order mass-transfer mechanism between the gas phase and the zeolite adsorption sites. This model fits when external mass transfer is controlling the process and can be reflected by the following equation[48,77]

$$q_t = q_e \left[1 - (\exp(-k_1 t))\right] \tag{9}$$

where k_1 (min^{-1}) is the rate constant of the pseudo-first-order equation, while q_t and q_e (mg g^{-1}) are defined as the amounts of adsorbed H_2S at time t (min) and at equilibrium time, respectively.

It was initially evolved to describe packed-bed dynamics under linear equilibrium conditions.[48] The advantage of this approximation lies in its simple formulas for unsteady-state diffusion in porous particles. That said, it has been developed solely for no-reaction occasions and cannot differentiate between the diffusing and the adsorbed phase, which are generally distinguishable for adsorption in porous materials. Notwithstanding, many works have used the PFO model to describe reaction, adsorption, and unsteady diffusion phenomena.[78]

The reaction step at pore surfaces can also be the controlling step for the system. In this respect, the mass-transfer parameter that is determined by diffusion and linear driving force kinetic models is substituted by a second-order reaction rate constant, k_2.[48] Thereby, in the case of pseudo-second-order (PSO) processes, the rate-limiting step may be chemisorption.[79] PSO can be expressed by the following equation[73,80]

$$q_t = \frac{k_2 q_e^2 t}{1 + k_2 q_e t} \tag{10}$$

where k_2 is the rate constant of PSO (g mg^{-1} min^{-1}) and q_t and q_e are the amounts of adsorbed H_2S at time t and at equilibrium (mg g^{-1}), respectively. The term $k_2 q_e^2$ denotes the initial adsorption rate.

As it can be seen in Table 4 and Figure 10, the Bangham model fits the adsorption data best as it demonstrates the

Table 4. Calculation of Kinetic Parameters

PFO	value	PSO	value
R^2	0.994	R^2	0.993
k_1 (min^{-1})	1.77×10^{-3}	k_2 (g mg^{-1} min^{-1})	1.4×10^{-7}
$q_{e,cal}$ (mg g^{-1})	377.1	$q_{e,cal}$ (mg g^{-1})	691.5
Weber–Morris	value	Bangham	value
R^2	0.975	R^2	0.997
k_{WM} (mg g^{-1} min$^{-0.5}$)	11.07	k_b (min^{-n})	1.02×10^{-3}
C	−43.89	n	1.28
		$q_{e,cal}$ (mg g^{-1})	195.5

highest R^2 value and a theoretically calculated H_2S uptake that is very close to the experimental one, which suggests that the adsorption of H_2S onto IMS was probably controlled by pore diffusion.[81] In other words, pore diffusion can be the rate-limiting step that determines the overall rate of the process, as is usually the case when microporous adsorbents are employed in physical adsorption processes.[48]

As pore diffusion was the rate-determining step of the process, probably due to the material's microporosity (also evidenced by the isotherms), one may hypothesize that the flow rate used in this study (100 mL min^{-1}) was high enough to minimize the influence of the external film of mass transfer.
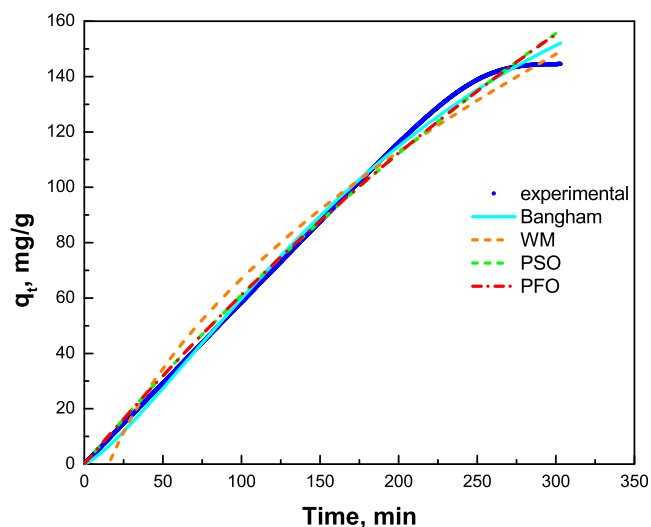
Figure 10. Adsorption kinetics of H_2S into IMS (25 °C, 3000 ppm of H_2S, 1 atm, flow rate 100 mL min^{-1}).

It can be assumed that in lower flow rates the contribution of external diffusion resistance would be more important and both external and internal mass-transfer resistance would be significant.[82]

Particle size is also crucial for adsorption kinetics, as the rate of the process depends inversely on particle size,[83,84] which means that by selecting a different particle size the mass-transfer zone (MTZ) can be narrowed. However, in this set of experiments, the mass-transfer zone was already narrow, which is, in principle, desirable for adsorbents intended for industrial use (the stated aim of our study).

Subsequently, the rate constants of the more suitable Bangham model, obtained at four different temperatures (Table 5), were used in the modified Arrhenius plot, as shown in Figure 11. The Arrhenius equation can be derived as follows[62]

$$k_b = A \exp(-E_a / R T) \tag{11}$$

Table 5. Calculation of k_b (Bangham Constant) for Four Different Temperatures

Kelvin	q_e (mg g^{-1})	k_b	R^2
298.15	195.5	1.02×10^{-3}	0.997
308.15	150.7	1.08×10^{-3}	0.997
323.15	107.7	1.52×10^{-3}	0.997
373.15	15.8	15.81×10^{-3}	0.999

The estimated activation energy for the H_2S adsorption process was 42.7 kJ mol^{-1}, and the pre-exponential factor was calculated to be 0.00212, by nonlinear methods ($R^2 = 0.995$).

2.3.3. Thermodynamic Studies. Thermodynamic parameters are crucial to verify the spontaneity and feasibility of the adsorption process as they afford important information to design an adsorption process. Typically, the thermodynamic parameters under consideration include heat of enthalpy ΔH^0, Gibbs free energy ΔG^0, and entropy ΔS^0. The equilibrium constant derived from K_d (coefficient distribution) was used to determine the Gibbs free energy changes.

The term of Gibbs free energy change can be determined from the following equation[85]
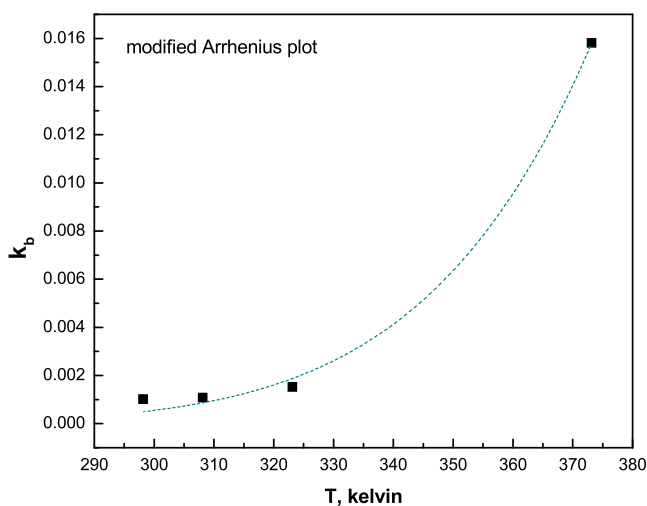
Figure 11. Effect of temperature on k_b (min^{-n}) Bangham's constant (modified Arrhenius plot).

$$\Delta G^0 = -R\,T\ln K_d \tag{12}$$

The temperature effect on K_d is denoted as follows[85]

$$\frac{\text{d}\ln K_d}{\text{d}T} = \frac{\Delta H^0}{R\,T^2} \tag{13}$$

Integrating eq 13 gives

$$\ln K_d = -\frac{\Delta H^0}{R\,T} + \frac{\Delta S^0}{R} \tag{14}$$

Multiplying eq 14 with the term RT and considering the form of eq 12 gives

$$\Delta G^0 = \Delta H^0 - T\,\Delta S^0 \tag{15}$$

K_d is defined as[62]

$$K_d = \frac{q_e}{C_e} \tag{16}$$

Consequently, using eqs 12 and 16, one can calculate the Gibbs free energy (Table 6).

**Table 6. Thermodynamic Parameters of the H$_2$S Adsorption Process**

Kelvin	K_d	ΔG^0 (kJ mol^{-1})
298.15	39.51	−9.11
308.15	31.52	−8.84
323.15	24.53	−8.60
373.15	5.88	−5.50

As mentioned above, four different adsorption temperatures (25, 35, 50, and 100 °C) were probed in this work, so ΔG^0 was calculated for each temperature. As presented in Table 6, the negative ΔG^0 values at given temperatures suggest the spontaneous nature of the adsorption and corroborate the feasibility of the adsorption process. Typically, when the ΔH^0 value is in the range of −80−400 kJ mol^{-1}, the adsorption process is dominated by chemisorption, while when the ΔH^0 value is in the range of −20−40 kJ mol^{-1}, physisorption predominates.[61]

The adsorption of IMS was more favorable at ambient temperature (25 °C) and the H$_2$S uptake gradually decreased upon increasing temperature, suggesting that the adsorbate–adsorbent interaction weakened. Therefore, higher temperatures did not promote H$_2$S adsorption; yet, a lower temperature was found to be adjuvant, which is also evident by ΔG^0 values obtained at four different temperatures (Table 6).

The calculations shown in Figure 12 were once again carried out by nonlinear methods ($R^2 = 0.946$), and the value of ΔH^0
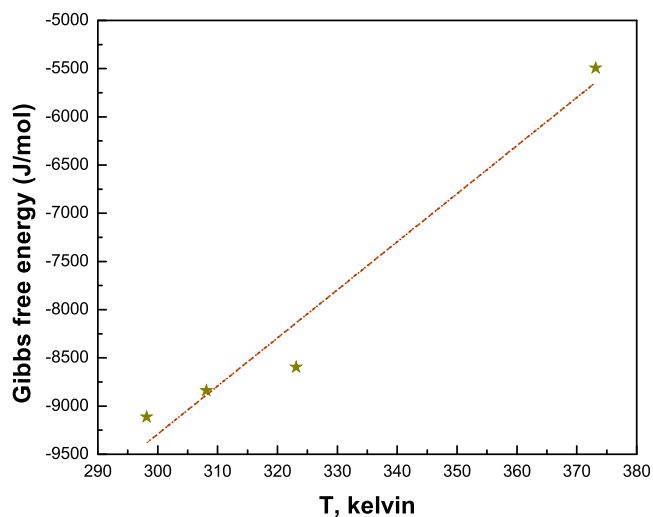
Figure 12. Gibbs free energy versus temperature.

was found to be −24.2 kJ mol^{-1}, suggesting that the adsorption process is an exothermic one (physisorption). The entropy change value ΔS^0 was −49.87 J mol^{-1} K^{-1}, indicating decreased randomness at the adsorbent/adsorbate interface and no significant changes in the internal structure of the adsorbent through the adsorption.[86]

3. CONCLUSIONS

In this study, a commercial molecular sieve, resembling a zeolitic structure with a morphology of cubic crystallites with a high surface area of 590 m^2 g^{-1}, was employed to capture H$_2$S from gas mixtures. The effects of temperature, H$_2$S inlet concentration, gas matrix, and adsorption/desorption cycles were investigated. Moreover, we tried to elucidate the equilibrium, kinetics, and thermodynamic parameters, with a view to shedding light on the mechanisms that govern the adsorption process.

It was found that increasing temperature resulted in decreased H$_2$S adsorption capacities, indicating that physisorption occurs.

In addition, increase in the initial H$_2$S concentration resulted in a decrease in the breakpoint, which is attributed to the effective pore diffusivity decrease on increasing the initial H$_2$S content.

Increasing CO$_2$ concentration negatively affects the desulfurization performance. However, the H$_2$S uptake remained relatively high, suggesting that this molecular sieve can be an alternative for selective H$_2$S physisorption.

Regeneration studies showed that reversible adsorption occurs, and the molecular sieve can be successfully reused for at least 15 cycles.

Data analysis showed that the Langmuir sorption isotherm can best describe the sorption behavior.

The desulfurization process on IMS follows the Bangham model, which signifies that the sorption kinetics are limited by pore diffusion.

The activation energy was calculated to be 42.70 kJ mol^{-1} (physisorption).

The thermodynamic studies revealed that the desulfurization process on IMS is a spontaneous and exothermic process, and physical adsorption is the predominant adsorption mechanism ($\Delta H^0 = -24.2$ kJ mol^{-1}).

4. EXPERIMENTAL SECTION

4.1. Selected Adsorbent for H$_2$S Removal. The adsorption runs were carried out using an industrial molecular sieve (the material is referred to as IMS throughout this manuscript) that was kindly supplied by Merck Group. The IMS is an alkali-metallic, silicon-aluminum material (sodium aluminum silicate). The physicochemical properties as supplied by Merck are presented in Table 7.

**Table 7. Physicochemical Properties of IMS**

property	value
melting point	<1600 °C
pH value	8−11
bulk density	700−750 kg m^{-3}
density	1.363 g dm^{-3}
shape	spherical
sphere diameter	0.9 nm
pore diameter	0.5 nm

According to Merck, IMS (product number: 1.05705.0250) is mainly used for the removal of different kinds of impurities from gases (i.e., H$_2$O, SO$_2$, CO$_2$, and C$_2$H$_4$). Properties such as porosity, crystallinity, morphology, and elemental composition were investigated during this study using N$_2$ porosimetry, X-ray diffraction, and scanning electron microscopy (SEM) along with EDX elemental analysis (see the section below).

4.2. Structural and Textural Characterization. Crystallinity was studied using X-ray diffraction (XRD) patterns, which were acquired using a D2 Phase$_{(R)}$ apparatus (Bruker, MA) with Cu Kα radiation ($\lambda = 1.5418$ Å). A voltage of 30 kV and an intensity of 20 mA with 2θ range of 10−100° and step size of 0.02° s^{-1} were used. A high-resolution 3Flex Micromeritics (Atlanta) porosimeter was used for studying the N$_2$ adsorption−desorption isotherms at cryogenic conditions (liquid nitrogen temperature 77 K). Before measurement, the adsorbent was outgassed at 150 °C overnight to remove any residual impurities. The Brunauer−Emmett−Teller (BET) method was employed to measure the surface area. Additionally, the pore size distribution was calculated, using the desorption branch of the N$_2$ isotherms, using the Barrett−Joyner−Halenda (BJH), Horvath−Kawazoe (HK), and nonlocal density functional theory (NLDFT) methods. Field-emission scanning electron microscopy (FESEM) coupled with energy-dispersive X-ray spectroscopy (FESEM-EDS) was employed using a JEOL JSM-7610F (Tokyo, Japan) for morphological and elemental analyses.

4.3. Experimental Apparatus. The adsorption tests were carried out in a fixed-bed quartz reactor (9 mm internal diameter and 400 mm length) under ambient pressure; a schematic representation of the test rig used is provided in Figure 13. The bed of the adsorbent (20 mm bed height) was built by packing 0.7 g of the material, supported on either side of the reactor by inert quartz wool. The bed geometry (h/D) was 2.22, where h stands for the height of the bed and D for the diameter. The temperature of the reactor was measured by a K-type thermocouple located in its center. The temperature of the reactor furnace, which could achieve a wide range of operating temperatures (up to 800 °C), was also controlled by a K-type thermocouple.
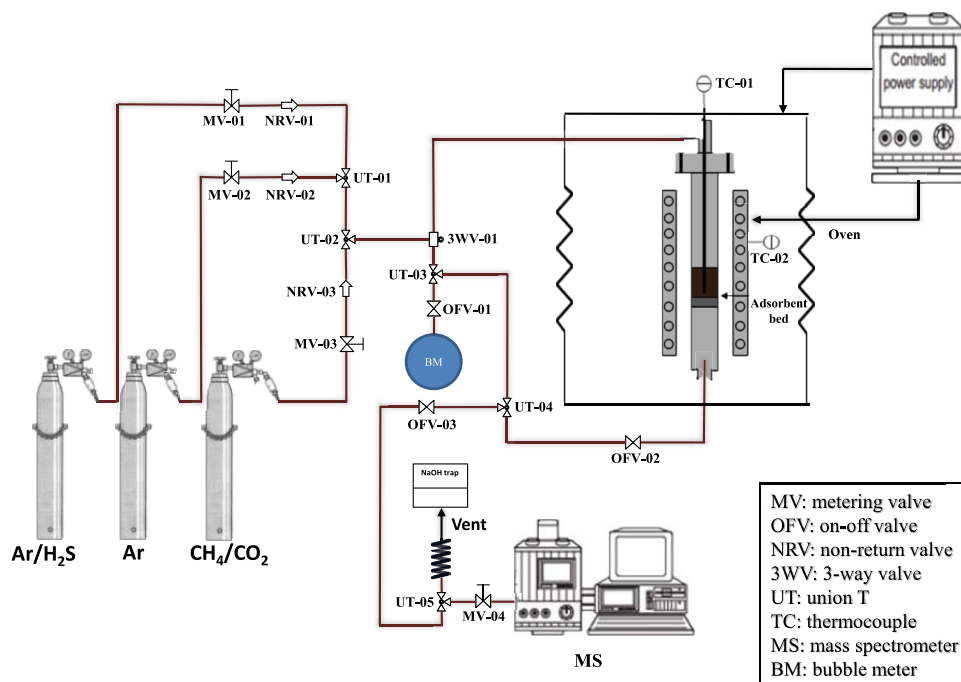
**Figure 13.** Experimental layout of H$_2$S adsorption on IMS.

The inlet gas mixture was prepared using 10 000 ppm of H_2S in Ar, which was diluted further with high-purity Ar (5.0), and when needed, with CO_2/CH_4. Gas flows were controlled by means of stainless steel (SS) metering valves, supplied by Parker. Gas flows were measured carefully using a bubble meter prior to the commencement of each experiment. Different H_2S concentrations (i.e., 200, 1000, 2000, 3000, 4000, 6000, 8000, and 10 000 ppm) were tested. For safety reasons, 15 m of plastic tubes that covered the two possible outlets (bubble meter and reactor's exit) were used, and the tail gas after the adsorption was treated with NaOH before discharge. All other pipelines and the fittings in the experimental apparatus were of stainless steel, which was treated with Sulfinert to prevent the adsorption of ppm levels of H_2S on the working surfaces.

The concentrations of Ar, H_2S, and CO_2/CH_4 in the gas mixtures were measured using a mass spectrometer (QMS 300 Prisma of Pferffer Group), which was able to perform an immediate and continuous monitoring.

4.4. Methodology. For the study of H_2S adsorption on the IMS, several breakthrough experiments were carried out at different experimental conditions. The parameters under consideration were temperature, inlet H_2S concentration, gas matrix (Ar, CO_2/CH_4), and regenerability.

Prior to the adsorptions tests, the molecular sieve was preheated in situ at 200 °C under a continuous flow of high-purity Ar (5.0) at a rate of 50 mL min^{-1} for 2 h to remove any moisture or residuals that may have been present. Subsequently, the reactor was cooled down to the desired temperature at which H_2S adsorption took place under 1 atm. The total flow rate was kept constant at 100 mL min^{-1} for all experiments. In addition to the runs carried out at room temperature, H_2S adsorption tests were also performed at 35, 50, and 100 °C.

To assess the effect of different parameters, starting from a reference condition, one parameter was changed at a time, while the others remained unchanged. The reference condition was a gas matrix of dry Ar gas containing H_2S at a concentration of 3000 ppm. The total flow rate was 100 mL min^{-1}. These initial experiments were carried out at ambient temperature and pressure. The adsorption experiments were halted when the system reached equilibrium and until the ratio C_t/C_0 became approximately 1 (Figure 14). The capacity of the bed (mg H_2S g^{-1} of sorbent) was determined by eq 17
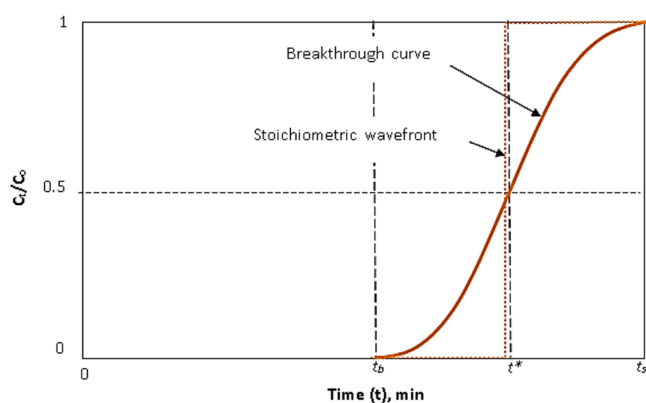
considering that the entire bed of the adsorbent approaches equilibrium ($C_t/C_0 = 1$).[87]

$$\mathrm{Cap}_{H_2S} = \frac{F_R\, C_0\, t^*}{W_{sorb}} - \frac{\epsilon\, \pi D^2\, L\, C_0}{4 W_{sorb}} \tag{17}$$

where t^* (min) is the time when the stoichiometric wavefront would leave the bed (Figure 14), F_R is the flow rate (mL min^{-1}), W_{sorb} is the weight of the sorbent (g), and C_0 is the concentration of H_2S in the bed exit.

Cap_{H_2S} is proportional to the area covered by the following integration (eq 18)

$$t_s = \int_{t=0}^{t=\mathrm{equilibrium}} (1 - C_t/C_0)\, dt \tag{18}$$

where t_s (min) is the time when the trailing end of the breakthrough curve leaves the bed (Figure 14), or to the usable capacity of the bed up to the breakpoint time t_b (eq 19) at an exit H_2S concentration reaching 5% of the feed gas concentration ($C_t/C_0 = 0.05$).[88]

$$t_b = \int_{t=0}^{t=\mathrm{breakpoint}} (1 - C_t/C_0)\, dt \tag{19}$$

The second term of eq 17 is a correction term, where ϵ refers to the bed void fraction, D is the bed diameter, and L is the bed length, which accounts for the nonadsorbed molecules remaining in the voids of the bed. However, this term was omitted as its amount was infinitesimal.

■ AUTHOR INFORMATION

Corresponding Author

   Maria A. Goula − *Laboratory of Alternative Fuels and Environmental Catalysis (LAFEC), Department of Chemical Engineering, University of Western Macedonia, GR-50100 Koila, Greece;* ⊙ orcid.org/0000-0002-6188-4095; Email: mgoula@uowm.gr

Authors

   Amvrosios G. Georgiadis − *Laboratory of Alternative Fuels and Environmental Catalysis (LAFEC), Department of Chemical Engineering, University of Western Macedonia, GR-50100 Koila, Greece*

   Nikolaos D. Charisiou − *Laboratory of Alternative Fuels and Environmental Catalysis (LAFEC), Department of Chemical Engineering, University of Western Macedonia, GR-50100 Koila, Greece*

   Safa Gaber − *Department of Mechanical Engineering, Khalifa University of Science and Technology, Abu Dhabi, UAE;* ⊙ orcid.org/0000-0002-6823-0465

   Kyriaki Polychronopoulou − *Department of Mechanical Engineering and Center for Catalysis and Separations, Khalifa University of Science and Technology, Abu Dhabi, UAE;* ⊙ orcid.org/0000-0002-0723-9941

   Ioannis V. Yentekakis − *Laboratory of Physical Chemistry & Chemical Processes, School of Environmental Engineering, Technical University of Crete, GR-73100 Chania, Greece;* ⊙ orcid.org/0000-0003-3502-8655

Complete contact information is available at:
https://pubs.acs.org/10.1021/acsomega.0c06157

Figure 14. Schematic of the adsorption wavefront and breakthrough curve in adsorption experiments.

Notes
The authors declare no competing financial interest.

ACKNOWLEDGMENTS

REFERENCES

(1) Charisiou, N. D.; Siakavelas, G.; Tzounis, L.; Sebastian, V.; Monzon, A.; Baker, M. A.; Hinder, S. J.; Polychronopoulou, K.; Yentekakis, I. V.; Goula, M. A. An in depth investigation of deactivation through carbon formation during the biogas dry reforming reaction for Ni supported on modified with CeO_2 and La_2O_3 zirconia catalysts. *Int. J. Hydrogen Energy* 2018, 43, 18955−18976.

(2) Charisiou, N. D.; Tzounis, L.; Sebastian, V.; Hinder, S. J.; Baker, M. A.; Polychronopoulou, K.; Goula, M. A. Investigating the correlation between deactivation and the carbon deposited on the surface of Ni/Al_2O_3 and $Ni/La_2O_3-Al_2O_3$ catalysts during the biogas reforming reaction. *Appl. Surf. Sci.* 2019, 474, 42−56.

(3) Yentekakis, I. V.; Goula, G. Biogas management: Advanced utilization for production of renewable energy and added-value chemicals. *Front. Environ. Sci.* 2017, 5, No. 42.

(4) Bareschino, P.; Mancusi, E.; Forgione, A.; Pepe, F. Biogas purification on Na-X Zeolite: Experimental and numerical results. *Chem. Eng. Sci.* 2020, 223, No. 115744.

(5) Capa, A.; García, R.; Chen, D.; Rubiera, F.; Pevida, C.; Gil, M. V. On the effect of biogas composition on the H_2 production by sorption enhanced steam reforming (SESR). *Renewable Energy* 2020, 160, 575−583.

(6) Ali, S.; Hua, B.; Huang, J. J.; Droste, R. L.; Zhou, Q.; Zhao, W.; Chen, L. Effect of different initial low pH conditions on biogas production, composition, and shift in the aceticlastic methanogenic population. *Bioresour. Technol.* 2019, 289, No. 121579.

(7) Papurello, D.; Boschetti, A.; Silvestri, S.; Khomenko, I.; Biasioli, F. Real-time monitoring of removal of trace compounds with PTR-MS: Biochar experimental investigation. *Renewable Energy* 2018, 125, 344−355.

(8) Bhoria, N.; Basina, G.; Pokhrel, J.; Kumar Reddy, K. S.; Anastasiou, S.; Balasubramanian, V. V.; AlWahedi, Y. F.; Karanikolos, G. N. Functionalization effects on HKUST-1 and HKUST-1/graphene oxide hybrid adsorbents for hydrogen sulfide removal. *J. Hazard. Mater.* 2020, 394, No. 122565.

(9) Shah, M. S.; Tsapatsis, M.; Siepmann, J. I. Hydrogen Sulfide Capture: From Absorption in Polar Liquids to Oxide, Zeolite, and Metal-Organic Framework Adsorbents and Membranes. *Chem. Rev.* 2017, 117, 9755−9803.

(10) Tsiotsias, A. I.; Charisiou, N. D.; Yentekakis, I. V.; Goula, M. A. The role of alkali and alkaline earth metals in the CO_2 methanation reaction and the combined capture and methanation of CO_2. *Catalysts* 2020, 10, No. 812.

(11) Truong, L. V.; Abatzoglou, N. A H_2S reactive adsorption process for the purification of biogas prior to its use as a bioenergy vector. *Biomass Bioenergy* 2005, 29, 142−151.

(12) Bandosz, T. J.; Bagreev, A.; Adib, F.; Turk, A. Unmodified versus caustics-impregnated carbons for control of hydrogen sulfide emissions from sewage treatment plants. *Environ. Sci. Technol.* 2000, 34, 1069−1074.

(13) Douvartzides, S. L.; Charisiou, N. D.; Papageridis, K. N.; Goula, M. A. Green diesel: Biomass feedstocks, production technologies, catalytic research, fuel properties and performance in compression ignition internal combustion engines. *Energies* 2019, 12, No. 809.

(14) Bagreev, A.; Rahman, H.; Bandosz, T. J. Study of H_2S adsorption and water regeneration of spent coconut-based activated carbon. *Environ. Sci. Technol.* 2000, 34, 4587−4592.

(15) Kikkinides, E. S.; Sikavitsas, V. I.; Yang, R. T. Natural Gas Desulfurization by Adsorption: Feasibility and Multiplicity of Cyclic Steady States. *Ind. Eng. Chem. Res.* 1995, 34, 255−262.

(16) Ozekmekci, M.; Salkic, G.; Fellah, M. F. Use of zeolites for the removal of H_2S: A mini-review. *Fuel Process. Technol.* 2015, 139, 49−60.

(17) Georgiadis, A. G.; Charisiou, N.; Yentekakis, I. V.; Goula, M. A. Hydrogen sulfide (H_2S) Removal via MOFs. *Materials* 2020, 13, No. 3640.

(18) Sisani, E.; Cinti, G.; Discepoli, G.; Penchini, D.; Desideri, U.; Marmottini, F. Adsorptive removal of H_2S in biogas conditions for high temperature fuel cell systems. *Int. J. Hydrogen Energy* 2014, 39, 21753−21766.

(19) van Rheinberg, O.; Lucka, K.; Köhne, H.; Schade, T.; Andersson, J. T. Selective removal of sulphur in liquid fuels for fuel cell applications. *Fuel* 2008, 87, 2988−2996.

(20) Cui, H.; Turn, S. Q.; Reese, M. A. Removal of sulfur compounds from utility pipelined synthetic natural gas using modified activated carbons. *Catal. Today* 2009, 139, 274−279.

(21) Mescia, D.; Hernández, S. P.; Conoci, A.; Russo, N. MSW landfill biogas desulfurization. *Int. J. Hydrogen Energy* 2011, 36, 7884−7890.

(22) Le-Minh, N.; Sivret, E. C.; Shammay, A.; Stuetz, R. M. Factors affecting the adsorption of gaseous environmental odors by activated carbon: A critical review. *Crit. Rev. Environ. Sci. Technol.* 2018, 48, 341−375.

(23) Georgiadis, A. G.; Charisiou, N. D.; Goula, M. A. Removal of hydrogen sulfide from various industrial gases: A review of the most promising adsorbing materials. *Catalysts* 2020, 10, No. 521.

(24) Bandosz, T. J. On the adsorption/oxidation of hydrogen sulfide on activated carbons at ambient temperatures. *J. Colloid Interface Sci.* 2002, 246, 1−20.

(25) Hamon, L.; Serre, C.; Devic, T.; Loiseau, T.; Millange, F.; Férey, G.; de Weireld, G. Comparative study of hydrogen sulfide adsorption in the MIL-53(Al, Cr, Fe), MIL-47(V), MIL-100(Cr), and MIL-101(Cr) metal-organic frameworks at room temperature. *J. Am. Chem. Soc.* 2009, 131, 8775−8777.

(26) Polychronopoulou, K.; Efstathiou, A. M. Effects of sol-gel synthesis on 5Fe-15Mn-40Zn-40Ti-O mixed oxide structure and its H_2S removal efficiency from industrial gas streams. *Environ. Sci. Technol.* 2009, 43, 4367−4372.

(27) Bülow, M.; Lutz, W.; Suckow, M. The mutual transformation of hydrogen sulphide and carbonyl sulphide and its role for gas desulphurization processes with zeolitic molecular sieve sorbents. *Stud. Surf. Sci. Catal.* 1999, 120 A, 301−345.

(28) Crespo, D.; Qi, G.; Wang, Y.; Yang, F. H.; Yang, R. T. Superior sorbent for natural gas desulfurization. *Ind. Eng. Chem. Res.* 2008, 47, 1238−1244.

(29) Kumar, P.; Sung, C. Y.; Muraza, O.; Cococcioni, M.; Al Hashimi, S.; McCormick, A.; Tsapatsis, M. H_2S adsorption by Ag and Cu ion exchanged faujasites. *Microporous Mesoporous Mater.* 2011, 146, 127−133.

(30) Khabazipour, M.; Anbia, M. Removal of Hydrogen Sulfide from Gas Streams Using Porous Materials: A Review. *Ind. Eng. Chem. Res.* 2019, 58, 22133−22164.

(31) Karge, H. G.; Raskó, J. Hydrogen sulfide adsorption on faujasite-type zeolites with systematically varied Si-Al ratios. *J. Colloid Interface Sci.* 1978, 64, 522−532.

(32) Cruz, A. J.; Pires, J.; Carvalho, A. P.; de Carvalho, M. B. Physical adsorption of H_2S related to the conservation of works of art: The role of the pore structure at low relative pressure. *Adsorption* 2005, 11, 569−576.

(33) Melo, D. M.; de Souza, J. R.; Melo, M. A.; Martinelli, A. E.; Cachima, G. H.; Cunha, J. D. Evaluation of the zinox and zeolite materials as adsorbents to remove H_2S from natural gas. *Colloids Surf., A* 2006, 272, 32−36.

(34) Barelli, L.; Bidini, G.; Micoli, L.; Sisani, E.; Turco, M. 13X Ex-Cu zeolite performance characterization towards H_2S removal for biogas use in molten carbonate fuel cells. *Energy* **2018**, *160*, 44−53.

(35) Alonso-Vicario, A.; Ochoa-Gómez, J. R.; Gil-Río, S.; Gómez-Jiménez-Aberasturi, O.; Ramírez-López, C. A.; Torrecilla-Soria, J.; Domínguez, A. Purification and upgrading of biogas by pressure swing adsorption on synthetic and natural zeolites. *Microporous Mesoporous Mater.* **2010**, *134*, 100−107.

(36) Tomadakis, M. M.; Heck, H. H.; Jubran, M. E.; Al-Harthi, K. Pressure-Swing Adsorption Separation of H_2S from CO_2 with Molecular Sieves 4A, 5A, and 13X. *Sep. Sci. Technol.* **2011**, *46*, 428−433.

(37) Micoli, L.; Bagnasco, G.; Turco, M. H_2S removal from biogas for fuelling MCFCs: New adsorbing materials. *Int. J. Hydrogen Energy* **2014**, *39*, 1783−1787.

(38) Yokogawa, Y.; Sakanishi, M.; Morikawa, N.; Nakamura, A.; Kishida, I.; Varma, H. K. VSC adsorptive properties in ion exchanged zeolite materials in gaseous and aqueous medium. *Procedia Eng.* **2012**, *36*, 168−172.

(39) Sigot, L.; Fontseré Obis, M.; Benbelkacem, H.; Germain, P.; Ducom, G. Comparing the performance of a 13X zeolite and an impregnated activated carbon for H_2S removal from biogas to fuel an SOFC: Influence of water. *Int. J. Hydrogen Energy* **2016**, *41*, 18533−18541.

(40) Yang, K.; Su, B.; Shi, L.; Wang, H.; Cui, Q. Adsorption Mechanism and Regeneration Performance of 13X for H_2S and SO_2. *Energy Fuels* **2018**, *32*, 12742−12749.

(41) Liu, X.; Wang, R. Effective removal of hydrogen sulfide using 4A molecular sieve zeolite synthesized from attapulgite. *J. Hazard. Mater.* **2017**, *326*, 157−164.

(42) Pourzolfaghar, H.; Ismail, M. H. *Developments in Sustainable Chemical and Bioprocess Technology*; Springer: US, 2013; pp 295−301.

(43) Fang, H. B.; Zhao, J. T.; Fang, Y. T.; Huang, J. J.; Wang, Y. Selective oxidation of hydrogen sulfide to sulfur over activated carbon-supported metal oxides. *Fuel* **2013**, *108*, 143−148.

(44) Agbonlahor, O. G.; Muruganathan, M.; Imamura, T.; Mizuta, H. Adsorbed Molecules as Interchangeable Dopants and Scatterers with a Van der Waals Bonding Memory in Graphene Sensors. *ACS Sens.* **2020**, *5*, 2003−2009.

(45) Jalan, V. M.; Wu, D. Desulfurization of hot coal gases by regenerative sorption. *AIP Conf. Proc.* **2008**, *70*, No. 457.

(46) Yaşyerli, S.; Ar, İ.; Doğu, G.; Doğu, T. Removal of hydrogen sulfide by clinoptilolite in a fixed bed adsorber. *Chem. Eng. Process.* **2002**, *41*, 785−792.

(47) Asaoka, S.; Yamamoto, T.; Kondo, S.; Hayakawa, S. Removal of hydrogen sulfide using crushed oyster shell from pore water to remediate organically enriched coastal marine sediments. *Bioresour. Technol.* **2009**, *100*, 4127−4132.

(48) Skodras, G.; Diamantopoulou, I.; Pantoleontos, G.; Sakellaropoulos, G. P. Kinetic studies of elemental mercury adsorption in activated carbon fixed bed reactor. *J. Hazard. Mater.* **2008**, *158*, 1−13.

(49) Ng, K. C.; Burhan, M.; Shahzad, M. W.; Ismail, A. B. A Universal Isotherm Model to Capture Adsorption Uptake and Energy Distribution of Porous Heterogeneous Surface. *Sci. Rep.* **2017**, *7*, No. 10634.

(50) Chowdhury, Z. Z.; Zain, S. M.; Rashid, A. K.; Rafique, R. F.; Khalid, K. Breakthrough curve analysis for column dynamics sorption of Mn(II) ions from wastewater by using *Mangostana garcinia* peel-based granular-activated carbon. *J. Chem.* **2013**, *2013*, No. 959761.

(51) Patton, A.; Crittenden, B. D.; Perera, S. P. Use of the linear driving force approximation to guide the design of monolithic adsorbents. *Chem. Eng. Res. Des.* **2004**, *82*, 999−1009.

(52) Wang, Y.; Wang, Z.; Liu, Y. Oxidation Absorption of Gaseous H_2S Using Fenton-Like Advanced Oxidation Systems. *Energy Fuels* **2018**, *32*, 11289−11295.

(53) Yuan, W.; Bandosz, T. J. Removal of hydrogen sulfide from biogas on sludge-derived adsorbents. *Fuel* **2007**, *86*, 2736−2746.

(54) Barelli, L.; Bidini, G.; de Arespacochaga, N.; Pérez, L.; Sisani, E. Biogas use in high temperature fuel cells: Enhancement of KOH-KI activated carbon performance toward H_2S removal. *Int. J. Hydrogen Energy* **2017**, *42*, 10341−10353.

(55) Olney, T. N.; Cann, N. M.; Cooper, G.; Brion, C. E. Absolute scale determination for photoabsorption spectra and the calculation of molecular properties using dipole sum-rules. *Chem. Phys.* **1997**, *223*, 59−98.

(56) Balsamo, M.; Cimino, S.; de Falco, G.; Erto, A.; Lisi, L. ZnO-CuO supported on activated carbon for H_2S removal at room temperature. *Chem. Eng. J.* **2016**, *304*, 399−407.

(57) de Oliveira, J. L. B.; Nascimento, B. O.; Gonçalves, D. V.; Santiago, R. G.; de Lucena, S. M. P.; de Azevedo, D. C. S.; Bastos-Neto, M. Effect of ultramicropores on the mechanisms of H_2S retention from biogas. *Chem. Eng. Res. Des.* **2020**, *154*, 241−249.

(58) Liu, J.; Wei, Y.; Li, P.; Zhao, Y.; Zou, R. Selective H_2S/CO_2 Separation by Metal-Organic Frameworks Based on Chemical-Physical Adsorption. *J. Phys. Chem. C* **2017**, *121*, 13249−13255.

(59) Xie, M.; Leung, A. K.; Ng, C. W. W. Mechanisms of hydrogen sulfide removal by ground granulated blast furnace slag amended soil. *Chemosphere* **2017**, *175*, 425−430.

(60) Sigot, L.; Ducom, G.; Germain, P. Adsorption of hydrogen sulfide (H_2S) on zeolite (Z): Retention mechanism. *Chem. Eng. J.* **2016**, *287*, 47−53.

(61) Raghav, S.; Kumar, D. Adsorption Equilibrium, Kinetics, and Thermodynamic Studies of Fluoride Adsorbed by Tetrametallic Oxide Adsorbent. *J. Chem. Eng. Data* **2018**, *63*, 1682−1697.

(62) Chung Lau, L.; et al. Adsorption Isotherm, Kinetic, Thermodynamic and Breakthrough Curve Models of H_2S Removal Using CeO_2/NaOH/PSAC. *Int. J. Petrochem. Sci. Eng.* **2016**, *1*, 36−44.

(63) Chowdhury, S.; Saha, P. Pseudo-second-order kinetic model for biosorption of methylene blue onto tamarind fruit shell: Comparison of linear and nonlinear methods. *Biorem. J.* **2010**, *14*, 196−207.

(64) El-Khaiary, M. I.; Malash, G. F.; Ho, Y. S. On the use of linearized pseudo-second-order kinetic equations for modeling adsorption systems. *Desalination* **2010**, *257*, 93−101.

(65) Xiao, Y.; Wang, S.; Wu, D.; Yuan, Q. Experimental and simulation study of hydrogen sulfide adsorption on impregnated activated carbon under anaerobic conditions. *J. Hazard. Mater.* **2008**, *153*, 1193−1200.

(66) Llorens, J.; Pera-Titus, M. A thermodynamic analysis of gas adsorption on microporous materials: Evaluation of energy heterogeneity. *J. Colloid Interface Sci.* **2009**, *331*, 302−311.

(67) Srivastava, V. C.; Mall, I. D.; Mishra, I. M. Competitive adsorption of cadmium(II) and nickel(II) metal ions from aqueous solution onto rice husk ash. *Chem. Eng. Process.: Process Intensification* **2009**, *48*, 370−379.

(68) Vasiliu, S.; Bunia, I.; Racovita, S.; Neagu, V. Adsorption of cefotaxime sodium salt on polymer coated ion exchange resin microparticles: Kinetics, equilibrium and thermodynamic studies. *Carbohydr. Polym.* **2011**, *85*, 376−387.

(69) Chen, F.-x.; Zhou, C.-r.; Li, G.-p.; Peng, F.-f. Thermodynamics and kinetics of glyphosate adsorption on resin D301. *Arab. J. Chem.* **2016**, *9*, S1665−S1669.

(70) Teng, H.; Hsieh, C. T. Influence of surface characteristics on liquid-phase adsorption of phenol by activated carbons prepared from bituminous coal. *Ind. Eng. Chem. Res.* **1998**, *37*, 3618−3624.

(71) Ayawei, N.; Ebelegi, A. N.; Wankasi, D. Modelling and Interpretation of Adsorption Isotherms. *J. Chem.* **2017**, *2017*, No. 3039817.

(72) Rahman, N.; Haseen, U. Equilibrium modeling, kinetic, and thermodynamic studies on adsorption of Pb(II) by a hybrid inorganic-organic material: Polyacrylamide zirconium(IV) iodate. *Ind. Eng. Chem. Res.* **2014**, *53*, 8198−8207.

(73) Kumar, K. V. Linear and non-linear regression analysis for the sorption kinetics of methylene blue onto activated carbon. *J. Hazard. Mater.* **2006**, *137*, 1538−1544.

(74) Ashori, E.; Nazari, F.; Illas, F. Adsorption of H_2S on carbonaceous materials of different dimensionality. *Int. J. Hydrogen Energy* **2014**, *39*, 6610−6619.

(75) Liu, X.; Zhang, L. Removal of phosphate anions using the modified chitosan beads: Adsorption kinetic, isotherm and mechanism studies. *Powder Technol.* **2015**, *277*, 112−119.

(76) Singh, T. P.; Majumder, C. B. Comparing fluoride removal kinetics of adsorption process from aqueous solution by biosorbents. *Asian J. Pharm. Clin. Res.* **2016**, *9*, 108−112.

(77) Mall, I. D.; Srivastava, V. C.; Agarwal, N. K. Adsorptive removal of Auramine-O: Kinetic and equilibrium study. *J. Hazard. Mater.* **2007**, *143*, 386−395.

(78) Kim, D. H. Linear driwing force formulas for unsteady-state diffusion and reaction in slab, cylinder and sphere catalyst. *AIChE J.* **2009**, *55*, 834−839.

(79) Reid, C. R.; Thomas, K. M. Adsorption of gases on a carbon molecular sieve used for air separation: Linear adsorptives as probes for kinetic selectivity. *Langmuir* **1999**, *15*, 3206−3218.

(80) LaCava, A. I.; Koss, V. A.; Wickens, D. Non-Fickian adsorption rate behaviour of some carbon molecular sieves. I. Slit-potential rate model. *Gas Sep. Purif.* **1989**, *3*, 180−186.

(81) Bilgili, M. S. Adsorption of 4-chlorophenol from aqueous solutions by xad-4 resin: Isotherm, kinetic, and thermodynamic analysis. *J. Hazard. Mater.* **2006**, *137*, 157−164.

(82) de Oliveira, L. H.; Meneguin, J. G.; Pereira, M. V.; da Silva, E. A.; Grava, W. M.; do Nascimento, J. F.; Arroyo, P. A. H_2S adsorption on NaY zeolite. *Microporous Mesoporous Mater.* **2019**, *284*, 247−257.

(83) Müller, B. R.; Calzaferri, G. Sorption properties of $Mo(CO)_6$ on thin Y-zeolite layers. *Microporous Mesoporous Mater.* **1998**, *21*, 59−66.

(84) Müller, B. R.; Calzaferri, G. Thin $Mo(CO)_6$-Y-zeolite layers: Preparation and in situ transmission FTIR spectroscopy. *J. Chem. Soc., Faraday Trans.* **1996**, *92*, 1633−1637.

(85) Li, G.; Shen, B.; Li, Y.; Zhao, B.; Wang, F.; He, C.; Wang, Y.; Zhang, M. Removal of element mercury by medicine residue derived biochars in presence of various gas compositions. *J. Hazard. Mater.* **2015**, *298*, 162−169.

(86) Doğan, M.; Alkan, M.; Demirbaş, Ö.; Özdemir, Y.; Özmetin, C. Adsorption kinetics of maxilon blue GRL onto sepiolite from aqueous solutions. *Chem. Eng. J.* **2006**, *124*, 89−101.

(87) Tan, K. L.; Hameed, B. H. Insight into the adsorption kinetics models for the removal of contaminants from aqueous solutions. *J. Taiwan Inst. Chem. Eng.* **2017**, *74*, 25−48.

(88) Al Mesfer, M. K.; Danish, M. Breakthrough adsorption study of activated carbons for CO_2 separation from flue gas. *J. Environ. Chem. Eng.* **2018**, *6*, 4514−4524.